

Imaging Stellar Radio Photospheres with the Next Generation Very Large Array

C.L. Carilli,¹ B. Butler,¹ K. Golap,¹, M.T. Carilli,² and S.M. White⁴

¹ *National Radio Astronomy Observatory, Charlottesville, VA, 22903; ccarilli@nrao.edu*

² *University of Colorado, Boulder, CO*

³ *Air Force Research Lab, Albuquerque, NM*

Abstract. We perform simulations of the capabilities of the Next Generation Very Large Array to image stellar radio photospheres. For very large (in angle) stars, such as red supergiants within a few hundred parsecs, good imaging fidelity results can be obtained on radio photospheric structures at 38 GHz employing standard techniques, such as disk model fitting and subtraction, with hundreds of resolution elements over the star, even with just the ngVLA-classic baselines to 1000 km. Using the ngVLA Rev B plus long baseline configuration (with baselines out to 9000 km, August 2018), we find for main sequence stars within ~ 10 pc, the photospheres can be easily resolved at 85 GHz, with accurate measures of the mean brightness and size, and possibly imaging large surface structures, as might occur on eg. active M dwarf stars. For more distant main sequence stars, we find that measurements of sizes and brightnesses can be made using disk model fitting to the u, v data down to stellar diameters ~ 0.4 mas in a few hours. This size would include M0 V stars to a distance of 15 pc, A0 V stars to 60 pc, and Red Giants to 2.4 kpc. Based on the Hipparcos catalog, we estimate that there are at least 10,000 stars that will be resolved by the ngVLA. While the vast majority of these (95%) are giants or supergiants, there are still over 500 main sequence stars that can be resolved, with ~ 50 to 150 in each spectral type (besides O stars). Note that these are lower limits, since radio photospheres can be larger than optical, and the Hipparcos catalog might not be complete. Our initial look into the Gaia catalog suggests these numbers might be pessimistic by a factor few.

1. Introduction

The field of stellar atmospheres, and atmospheric activity, has taken on new relevance in the context of the search for habitable planets, due to the realization of the dramatic effect 'space weather' can have on the development of life (Osten et al. 2018; Triglio et al. 2018). Observations at radio wavelengths provide some of the most powerful probes of exo-space weather, including: (i) high brightness coherent processes, such as masers associated with outflows in forming stars, (ii) non-thermal coherent and incoherent gyro-synchrotron emission due to magnetic activity in stellar coronae, and (iii) thermal emission from extreme mass loss events, such as novae (Gudel 2002; Linford et al. 2018).

In this article, we consider the more quiescent properties of stellar radio photospheres, namely, the thermal emission from the $\tau \sim 1$ surface of the photospheres

of stars of different types. The size of stars, as measured by their stellar radio photospheres, is a strong function of wavelength, since the free-free optical depth drops quickly with frequency ($\propto \nu^{-2.1}$). Hence, radio observations over a range in frequencies provide a tomographic image of the density and temperature structure of the transition from the optical photosphere to the chromosphere. For giant stars, the radio photosphere will be larger, and typically cooler, than the optical photosphere at long wavelengths, and approach the optical photospheric size and temperature at shorter wavelengths. For instance, in red super-giants, the radio photospheres at ~ 6 cm are typically $7\times$ larger, and $3\times$ cooler, than the optical photosphere, while at ~ 1 mm the radio and optical photospheric temperatures and sizes are comparable to within $\leq 30\%$ (Lim et al. 1998; O’Gorman et al. 2015, 2017; Harper et al. 2013). For main sequence stars, there should be closer correspondance between radio and optical photospheric sizes, although even in these cases, at cm and mm wavelengths the stellar atmospheres can become optically thick in the chromosphere, which would enhance temperatures by a few thousand Kelvin (eg. the Sun has a brightness temperature at 100 GHz of 7300 K(White et al. 2017)).

Of particular interest is the question of the end-of-life mass loss in red giants and supergiants through strong winds. Current observations suggest elevated atmospheres, with substantial large-scale temperature structure, heated by sound or Alfvén waves driven by large convective cells bubbling-up from the stellar interior (Lim et al. 1998; O’Gorman et al. 2015, 2017; Harper 2018; Matthews & Claussen 2018). For Solar-type and lower mass main sequence stars, recent interest has focused on atmospheric conditions that can drive strong winds, leading to star-planet magnetic interactions, possibly triggering auroral radio emission (Trigilio et al. 2018; Fichtinger et al. 2017; Hallinan et al. 2015).

To date, direct imaging of stellar radio photospheres has been limited to a handful of the largest, closest stars, such as red giants, super-giants, and AGB stars (Lim et al. 1998; Vlemmings et al. 2017; O’Gorman et al. 2013; Matthews & Claussen 2015). Likewise, detection of thermal emission from nearby solar-type main sequence stars is just possible with deep observations with the JVLA and ATCA (Villadsen et al. 2014; O’Gorman et al. 2017), but imaging is certainly impossible with current facilities. The situation is similar in the optical and near-IR, with a moderate number of large, hot stars resolved through optical interferometry or direct imaging with HST (Boyajian et al. 2015; Monnier, J. et al. 2007; Gilliland & Dupree 1996; Mozurkewich et al. 2003). For optical interferometers, structure is typically inferred through model fitting of interferometric closure quantities (Monnier 2003; Defrere et al. 2018), although hybrid closure-imaging approaches are being explored with the new VLTI (Montargé et al. 2018).

The ‘Next Generation Very Large Array’ (ngVLA) opens a new window on stellar radio photospheres, through sub-milliarcsecond resolution at up to 90 GHz with sub- μ Jy sensitivity (McKinnon et al. 2016; Carilli et al. 2015; Selina & Murphy 2017). The ngVLA rms brightness sensitivity in one hour at 85 GHz and 0.4 mas resolution is ~ 1000 K. There are thousands of stars with sizes larger than 0.4 mas, with brightness temperatures above a few thousand Kelvin at 90 GHz. These include nearby main sequence stars, and more distant giants and supergiants. We investigate the ability of the ngVLA to provide high fidelity images of the radio photospheres of larger (in angle) stars, and to determine sizes and flux densities for sub-mas stars.

2. Configuration, Model, and Process

We employ the newly accepted ngVLA configuration (August 2018). This configuration includes the original ngVLA Rev B configuration distributed across the US Southwest and Mexico. The Rev B configuration includes 214 antennas of 18 meter diameter, to baselines up to 1000 km (Carilli & Erickson 2018; Selina & Murphy 2017). The new ngVLA configuration includes 30 more antennas distributed to baselines of 9000 km, including clusters of two to three antennas at sites such as Hawaii and St. Croix.

We employ the *SIMOBSE* task within CASA to generate u, v data sets. Instructions on how this is done are found on the ngVLA web page.

The ngVLA has a highly centrally condensed antenna distribution. The naturally weighted beam for this centrally condensed distribution leads to a very non-Gaussian PSF, with two skirts extending to $10\times$ the nominal full resolution of the longest baselines at the 50% to 20% level, and $100\times$ the full resolution at the 20% to 10% level, for just the Rev B array alone. This PSF problem becomes an order of magnitude more severe when including the longer baselines, in terms of the relative angular size of the PSF 'spike' corresponding to the longest baselines vs. the skirts. These prominent skirts represent the major challenge when trying to image complex structure. The imaging process entails a balance between sensitivity and synthesized beam shape, using visibility tapering and Briggs robust weighting (Carilli et al. 2018; Cotton & Condon 2017; Carilli 2017, 2016). In all cases we employed the *CLEAN* algorithm with Briggs weighting, and adjusted the robust parameter and u, v -taper to give a reasonable synthesized beam and noise performance.

We employ a template stellar disk model that includes a few large cold and hot spots at the $\pm 10\%$ level (Fig 1a). Such spots have been seen on the radio photospheres of giant and supergiant stars. Such large structures are not present on most main sequence stars, but they provide some 'test structures' that exercise the imaging algorithms at high resolution. Moreover, active stars, such as M-dwarves, may have large temperature structures, such as giant sunspot regions. We then adjust the star size and mean brightness temperature according to the stellar types and assumed distance. We emphasize that the models below are not meant to be accurate reproductions of a specific star, just representative.

The new long baselines extend from 1000 km to 9000 km. The longest baselines that include correlation to the ngVLA core are about 5000 km (eg. Socorro to Hawaii). Beyond that, only outer stations are involved in the cross correlation, and we will show that the sensitivity drops dramatically beyond 5000 km baselines, as expected.

3. Results

3.1. Betelgeuse (α Orionis) at 38 GHz

Betelgeuse (α Orionis, J0555+0724, spectral type M1 Ia, Mass = $11.7 M_{\odot}$), is a red supergiant at a distance of 222 pc. For the Betelgeuse-like model, we adopt parameters for the radio photosphere guided by existing observations at 22 GHz to 43 GHz from the VLA (Lim et al. 1998; O'Gorman et al. 2017). The model has a diameter of 100 mas and a total flux density of 21.7 mJy at 1 cm wavelength. The implied mean brightness temperature is about 3000 K. The model includes large cold and hot spots with Gaussian profiles, with sizes (FWHM) up to 20% of the stellar diameter, and

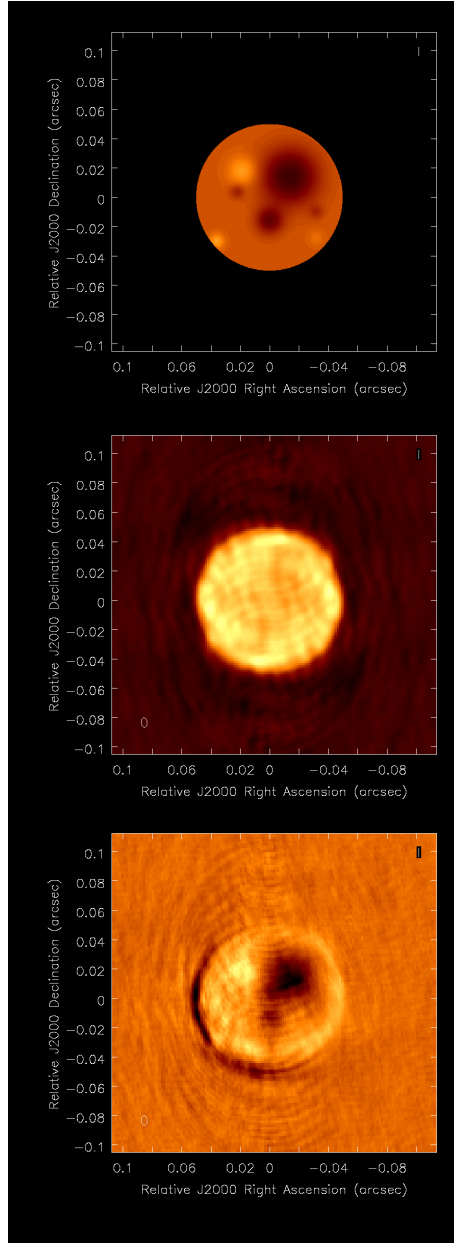


Figure 1. Images of Betelgeuse at 38 GHz. Top: the input model, including cold and hot spots of peak magnitude $\sim \pm 12\%$. Center: The ngVLA image at $6.5\text{mas} \times 4.0\text{mas}$ resolution, for a 4 hour synthesis. The rms noise is $0.51 \mu\text{Jy beam}^{-1}$, and the peak surface brightness is $0.1 \text{ mJy beam}^{-1}$. Bottom: Image with the ngVLA, after fitting for a disk model, and subtracting the model from the visibilities. The rms noise is $0.25 \mu\text{Jy beam}^{-1}$, and the peak surface brightness is $7.8 \mu\text{Jy beam}^{-1}$.

peak deviations from the mean of $\pm 12\%$, qualitatively consistent with radio imaging of Betelgeuse.

The model is shown in Figure 1a. We simulated a 4 hour observation of this model with the ngVLA at 38 GHz (Figure 1b). For imaging, we adopt Briggs weighting with $\text{robust} = -0.5$, and we use a multiscale clean with a loop gain of 0.03 to mitigate the CLEAN instability. The resulting image has an rms noise of $0.6 \mu\text{Jy beam}^{-1}$, and the synthesized beam has a $\text{FWHM} = 6.5 \text{ mas} \times 4.0 \text{ mas}$. The disk is imaged at high signal to noise, however, the hot and cold spots are only marginally perceptible. There is a depression at the position of the largest cold spot of $\sim 15\%$, but the overall impression is that of an edge-brightened disk. This result is a well known issue with interferometric imaging of objects with relatively flat brightness distributions and hard edges, such as the disks of planets in our Solar system (de Pater et al. 2016). The result is due to the natural tendency for an interferometer to enhance edges and sharp gradients in images, and the general CLEAN instability for diffuse sources (Cornwell 2008).

In the case of Solar system planets, the standard analysis technique is to perform disk model fitting to the visibilities, then subtract the disk model from the u, v data, to look for under-lying structures (de Pater et al. 2016). We have performed such an analysis on the Betelgeuse simulation. The results from the u, v -model fit are listed in Table 1. The residual image after model subtraction from the visibilities is shown in Figure 1c. The model fit provides an accurate realization of the mean disk, both in terms of size and total flux density, to better than 1%. The residual image shows the more prominent hot and cold spots, with magnitudes within 20% of the expected deviations. One artifact of the model and fitting process is that the largest cold spot is significant enough to perturb the central position of the fit. Even a $\sim 0.5\%$ position shift (relative to the stellar diameter), will lead to sharp positive/negative edges in the residual image.

Table 1. u, v Fitting Results

Star	Max Baseline $\times 10^8 \lambda$	S_{mod} mJy	D_{mod} mas	S_{fit} mJy	D_{fit} mas
α Orionis 38 GHz	1.3	21.7	100	21.6 ± 0.2	100.6 ± 0.5
α Can Maj 85 GHz	3.0	1.63	6.0	1.6295 ± 0.0002	$6.039 \pm 0.005 \times 6.042 \pm 0.003$
α Can Maj 85 GHz	–	1.63	6.0	1.6295 ± 0.0002	$6.040 \pm 0.005 \times 6.043 \pm 0.003$
θ Leonis 85 GHz	3.0	0.0255	0.723	0.0251 ± 0.00077	$0.58 \pm 0.41 \times 0.61 \pm 0.12$
θ Leonis 85 GHz	–	0.0255	0.723	0.0251 ± 0.00075	$0.56 \pm 0.17 \times 0.63 \pm 0.08$
A2 V at 100 pc 85 GHz	–	0.0064	0.36	0.0063 ± 0.0004	$0.45 \pm 0.14 \times 0.33 \pm 0.10$

3.2. Sirius (α Canis Majoris) at 85 GHz

Sirius is the brightest star in the sky in the optical (α Canis Majoris, J0645-1642), at a distance of 2.6 pc from Earth. It is a binary system, with the brighter star being a hot, $2 M_{\odot}$, main sequence star of spectral type A0, and the second star being a $1 M_{\odot}$ white dwarf. We focus on the A0 star.

For the radio model of a Sirius-like star, and subsequent analyses below, we adopt the parameters of the optical photosphere, in terms of diameter and brightness temperature, since the radio and optical photospheres for hot main sequence stars at 85 GHz are likely to be similar at the $\sim 30\%$ level, in size and brightness (White et al. 2018). We feel this assumption is conservative, in that the radio photospheres could be larger.

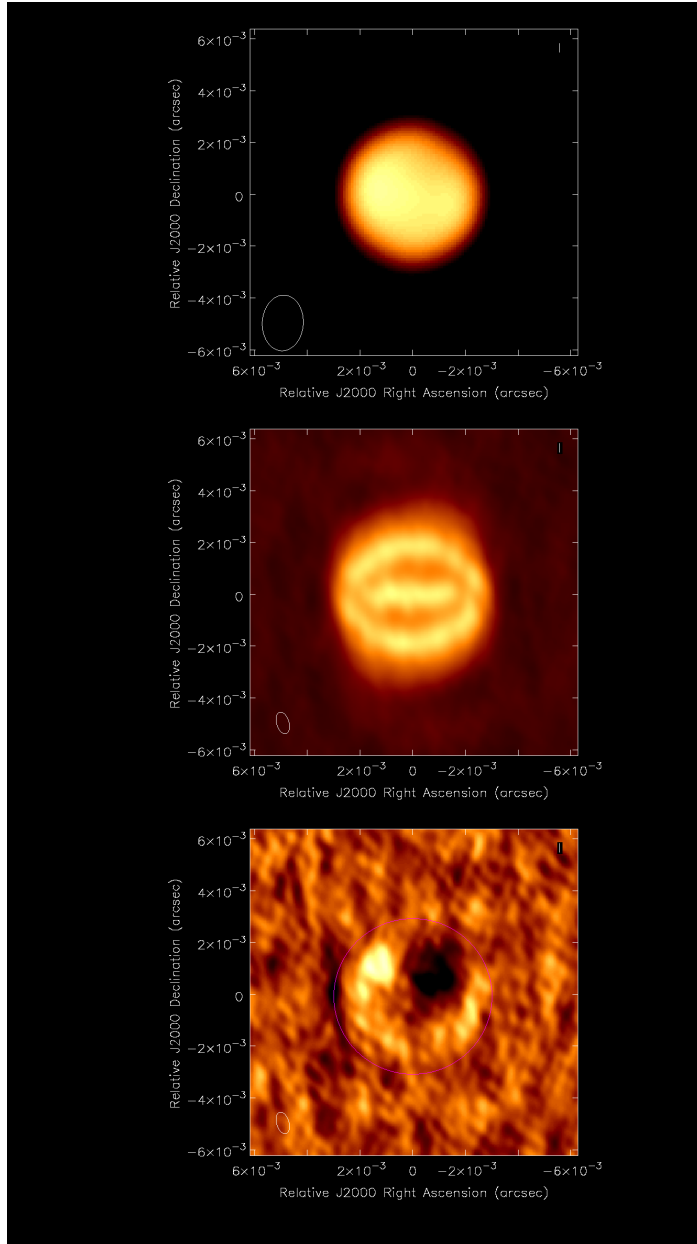


Figure 2. Top: Image of Sirius with the ngVLA for a 16 hour synthesis, made using u, v -weighting appropriate for the original Rev B configuration (1000 km maximum baseline). The resolution is $2.1\text{mas} \times 1.6\text{mas}$ and the $\text{rms} = 0.6 \mu\text{Jy beam}^{-1}$. Middle: Image of Sirius with u, v -weighting that incorporates the longer baselines. The resolution is $0.85\text{mas} \times 0.47\text{mas}$ and the $\text{rms} = 0.5 \mu\text{Jy beam}^{-1}$. Bottom: Image of Sirius with the same resolution as (b), after fitting for a disk model and subtracting the model from the u, v data. The pink circle shows roughly the position of the stellar disk. The peak on the image is $3.5 \mu\text{Jy beam}^{-1}$. (Note: please refer to Figure 1a for the model structure, scaled accordingly).

In this model, the angular diameter is 6 mas and the total flux density at 85 GHz is 1.63 mJy. The mean brightness temperature is about 9000 K. We incorporate the same stellar structure as in Section 3.1 (hot and cold spots). Such structures are unlikely in hot main sequence stars, but they allow us to explore the imaging capabilities of the array at the highest resolutions.

We simulate a 16 hour observation at 85 GHz with the Rev B configuration plus the long baselines. We first image with a taper appropriate to the scales of the Rev B baselines only: $R = -1.3$, a cell size of 0.1 mas, and an outer u, v -taper of 1.4 mas. The resulting image is shown in Figure 2a. The beam FWHM is $2.1 \text{ mas} \times 1.6 \text{ mas}$, and the rms is $0.6 \mu\text{Jy beam}^{-1}$ (the Naturally weighted theoretical noise is $0.2 \mu\text{Jy beam}^{-1}$). The resulting image shows a resolved star, but the resolution is inadequate to isolate any region clearly. There may be a depression at the location of the biggest cold spot, but again, the image is not conclusive.

We then image with a taper more appropriate for the longer baselines: $R = -1.3$, cell size of 0.05 mas, and an outer u, v -taper of 0.35 mas. The resulting synthesized beam FWHM is $0.85 \text{ mas} \times 0.47 \text{ mas}$, and the image noise is about $0.5 \mu\text{Jy beam}^{-1}$. Figure 2b shows the resulting image. The structure is clearly dominated by imaging artifacts.

We perform a similar disk u, v -model fitting and subtraction as in Section 3.1. The resulting image of the residuals is shown in Figure 2c, using the same weighting as is used in 2b. There is a reasonable indication of both the primary cold and hot spots, at levels within 30% of the expected values relative to the mean disk brightness, and even marginal evidence for the next lowest cold spot.

The results for the disk fitting to the visibilities are given in Table 1. We performed two fits: one using baselines from the original Rev B configuration out to 1000 km ($3e8 \times \lambda$), and the second using all the long baselines (out to 9000 km). In this case, the results are much the same, since the star is 6 mas in diameter, and the resolution of even the Rev B baselines is a factor few smaller than this.

3.3. θ Leonis at 85 GHz

We next consider a model of a hot main sequence star at a distance 20 times that of Sirius, and determine how well the stellar properties can be determined in a one hour synthesis, appropriate for surveys of large numbers of stars. We adopt the parameters comparable to those of θ Leonis, a $2.5 M_{\odot}$ A2 V star at a distance of 51 pc (J1114+1525). The model in this case has a total flux density at 85 GHz of $25.5 \mu\text{Jy}$, and a diameter of 0.723 mas. We simulate a 1 hour observation at 85 GHz using the Rev B plus long baseline configuration. The resulting image is shown in Figure 3. We use $R = -1.0$ and an outer taper of 0.35 mas. The beam FWHM = $0.84 \text{ mas} \times 0.62 \text{ mas}$, and the noise is about $2.0 \mu\text{Jy beam}^{-1}$. The resulting image is shown in Figure 3a.

More relevant than direct imaging in this case is u, v model fitting. Table 1 shows disk modeling fitting results, again using baselines appropriate for the Rev B configuration only, and then including the long baselines. In this case, the total flux density is well fit by both short and long baseline fits, but the errors on the diameters are significantly lower when including the longer baselines.

Figure 4 shows a radial binning of the Real part of the visibilities vs u, v -distance, plus the model visibilities. The Rev B only configuration does not reach the first null in the visibility function. The longer baselines sample the first three nulls at reasonable signal to noise, out to 1.4×10^9 wavelengths (= 5000 km). Beyond that, the sensitivity

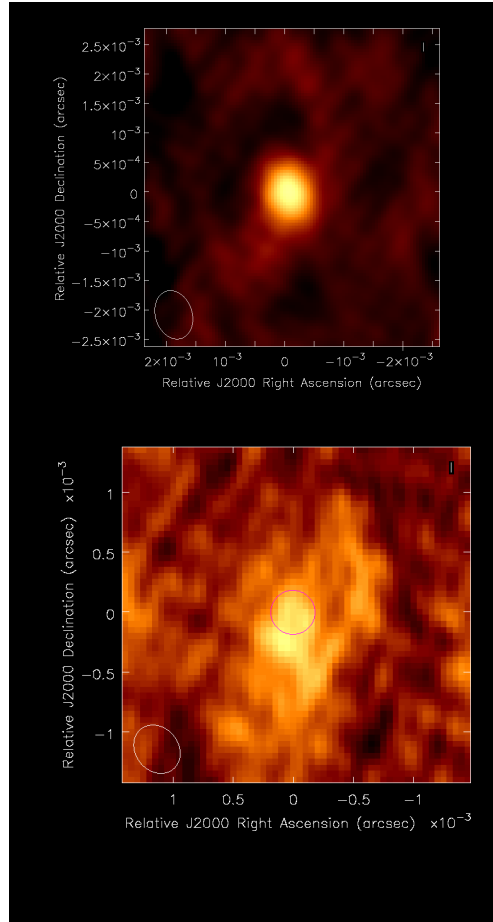


Figure 3. Top: Image of θ Leonis with the Rev B plus long baseline configuration of August, 2018, for a one hour synthesis. The resolution is $0.84 \text{ mas} \times 0.62 \text{ mas}$ and the rms = $2 \mu\text{Jy beam}^{-1}$. The peak on the image is $25 \mu\text{Jy beam}^{-1}$. Bottom: Image of an A2 V star at a distance of 10 pc using the Rev B plus long baseline configuration of August, 2018, for a 4 hour synthesis. The resolution is $0.43 \text{ mas} \times 0.36 \text{ mas}$ and the rms = $0.7 \mu\text{Jy beam}^{-1}$. The peak in the field is $3.6 \mu\text{Jy beam}^{-1}$. The circle shows the model photosphere position and size.

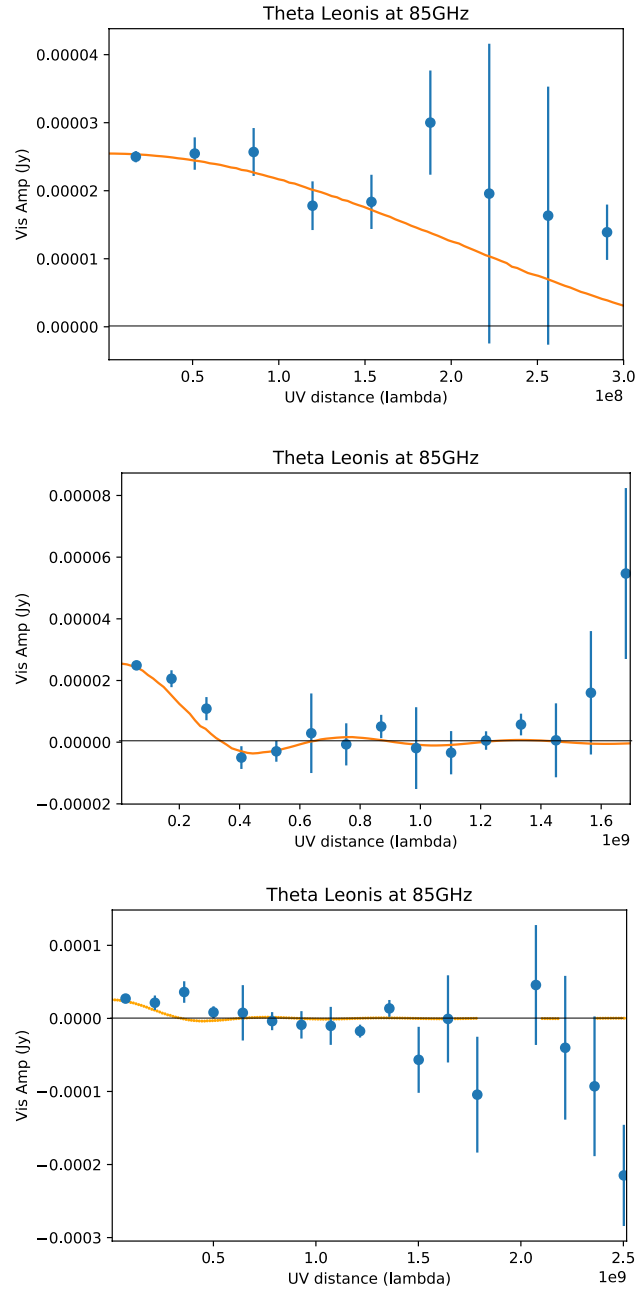


Figure 4. Azimuthally averaged Real part of the visibility curve for θ Leonis at 85 GHz. Points are the measurements for a 4 hour synthesis with the ngVLA-classic baselines to 1000 km (top) and the Rev B plus long baseline configuration truncated at about 5000 km (middle), and at 9000 km (bottom). Beyond about 5000 km, the measurements become very noisy since the large number of antennas in the Core and Plains no longer contribute.

drops dramatically. This sensitivity drop is due to the fact that only the outer antennas are involved in the cross correlation, and the Core and Plains antennas no longer contribute.

3.4. An A2 V Star at 100 pc: limiting case

To test the limits of the array, we model a hot main sequence star as above (A2 V star), but now at a distance of 100 pc, or 40 times further than Sirius. We simulate a 4 hour synthesis at 85 GHz. The total flux density in the model is $6.4 \mu\text{Jy}$, and the stellar diameter is 0.36 mas. We make an image using $R = -1.0$, $\text{taper} = 0.15 \text{ mas}$, and a cell size of 0.05 mas. The resulting resolution is 0.4 mas and rms noise is $0.70 \mu\text{Jy}$ (vs. $0.36 \mu\text{Jy}$ Naturally weighted theoretical noise). The resulting image is shown in Fig 3b. There is a fuzzy source at the expected position, but determining the size and total flux density from such an image is problematic, and disk fitting to the visibilities is the only viable method.

The results for disk fitting to the visibilities are again given in Table 1 using the full array. We find that the flux density is well determined ($\geq 10\sigma$), and the diameter is fit to $\sim 3\sigma$. We consider this the limiting case for determining stellar properties with the ngVLA.

Table 2. Hipparcos Stars > 0.4 mas, Dec > -40°

	I	II	III	IV	V	Total
O	6	1	0	0	2	9
B	114	77	81	55	61	388
A	35	32	105	118	61	351
F	55	47	148	245	159	654
G	67	106	1120	351	107	1751
K	55	117	5351	227	104	5854
M	27	32	1039	2	44	1144
Total	359	412	7884	998	538	10151

3.5. Number of Stars

Based on the simulations above, we adopt an extreme limiting case for determining stellar parameters of: a 1σ limit in 1hr of $1.4 \mu\text{Jy beam}^{-1}$ at 85 GHz and 0.4 mas stellar size. This limit implies an rms brightness temperature limit of 1500 K. M-type stars have optical photospheric temperatures of ~ 3000 to 4000 K, which would be at the limit of detection at this resolution. However, as mentioned above, at cm and mm wavelengths, the stellar atmospheres of main sequence stars can become optically thick in the chromosphere, which would enhance temperatures by a few thousand Kelvin. A size of 0.4 mas corresponds to the diameter of an M0 V star (optical radius of $0.6R_\odot$) at a distance of 15 pc. For A0 V stars (radius of $2.5R_\odot$), the distance is 60 pc. Red giant stars (radii of order $100R_\odot$), could be resolved to 2.5 kpc.

The Hipparcos catalog has a detailed listing of stellar spectral type, luminosity class, and distance (Perryman et al. 1997). From these quantities, we derive angular sizes using standard relationships for stellar optical photospheric diameters from Allen's Astrophysical Quantities (Table 15.8). We then select for stars above -40°

Dec, with angular diameters > 0.4 mas. The results as a function of spectral type and luminosity class, are given in Table 2. The total number of stars evaluated was 32886 (meaning stars with fully specified spectral type and luminosity class, not Carbon stars, and above -40° Dec¹). Of these, 10151 are larger than 0.4 mas. The vast majority of the resolved stars are in the Giant or Supergiant class (9613 or 95% in class IV or lower). Yet there are still more than 500 main sequence stars (class V), that could be resolved by the ngVLA, with ~ 50 to 150 in each spectral type, except for the O stars.

For those interested in making direct comparisons to the Sun, there are 43 'Solar-type' stars ($B - V$ color index between 0.65 and 0.67), and 145 'Solar-analog' stars ($B - V$ color index between 0.62 and 0.71), that could be resolved by the ngVLA.

We note that these are lower limits, since the radio photospheres can be substantially larger than the optical photospheres, in particular in Giants and Supergiants, or hotter, in the case of main sequence stars. Additionally, the Hipparcos catalog is much smaller than the new GAIA survey (Andrae et al. 2018). However, by definition, the larger (in angle) stars of a given type/class will also be closer, and hence brighter and more likely to be in both catalogs.

For completeness, we have also searched the Gaia catalog. Of the almost 1.7 billion stars in that catalog, there are 77 million which have both effective temperature and radius cataloged, of which 54 million are above -40° Dec. Based on the radii and distances in the catalog, we find that there are about 40,000 stars larger than 0.4 mas and Dec $\geq -40^\circ$. Of these, we estimate that 246 are "solar analogs", meaning with tabulated radius and temperature within 30% Solar. The Gaia catalog does not contain information about spectral type or luminosity class, so no table similar to Table 2 for the Hipparcos catalog can be made, nor does it contain values for $B - V$, so we cannot define 'solar-type' stars in quite the same way as for Hipparcos.

4. Conclusions

The ngVLA will transform the field of stellar radio photospheres, allowing for imaging and parameter estimation of thousands of main sequence and giant stars. Such studies are directly relevant to determining the structure of stars in the key transition region from the optical photosphere to the chromosphere – the regions powering exo-space weather phenomena.

For very large (in angle) stars, such as red supergiants within a few hundred parsecs, good fidelity results can be obtained, with many resolution elements across the star. Even the closer main sequence stars (within ten parsecs or so), can be resolved and imaged, although with reduced image fidelity. In these cases, large scale temperature structures are not expected on the radio photospheres, and the primary physical parameters of diameter and brightness will be well constrained.

Using the Hipparcos catalog measurements of stellar spectral type, luminosity class, and distance for over 100,000 stars, we estimate that there are at least 10,000 stars that will be resolved by the ngVLA. While the vast majority of these (95%) are giants or supergiants, there are still over 500 main sequence stars that can be resolved, with ~ 50 to 150 of each spectral type (besides O stars). Note that these are lower limits,

¹The 32886 was out of a total number of stars in the catalog of 118218, of which 91488 are above -40° Dec

since radio photospheres can be larger than optical, and the Hipparcos catalog might not be complete. An initial investigation of the Gaia catalog suggests these numbers may be pessimistic by a factor of a few.

Acknowledgments. The National Radio Astronomy Observatory is a facility of the National Science Foundation operated under cooperative agreement by Associated Universities, Inc.

References

- Andrae, R., Fouesneau, M., Creevey, O. et al. 2018, A& A, in press
 Boyajian, T., von Braun, K., Feiden, G. A., et al. 2015, MNRAS, 447, 846
 Carilli, C. & Erickson, A. 2018, ngVLA Memo No. 41
 Carilli, C. et al. 2018, ngVLA Memo No. 35
 Carilli, C. 2017, ngVLA Memo No. 16
 Carilli, C. 2016, ngVLA Memo No. 12
 Carilli, C. et al. 2015, ngVLA Memo No. 5
 Cornwell, T. 2008, IEEE Journal of Selected Topics in Signal Processing, 2, 793
 Cotton, W. & Condon, J. 2017, ngVLA Memo No. 30
 Defrere, D., Absil, O., Berger, J.-P., et al. 2018, Experimental Astronomy, in press
 Fichtinger, B., Gudel, M., Mutel, R. et al., 2017, A & A, 599, 127
 Gilliland, R. & Dupree, A. 1996, ApJ, 436, L29
 Gudel, M 2002, ARAA, 40, 217
 Hallinan, G., Littlefair, S., Cotter, G. et al. 2015, Nature, 523, 568
 Harper, G. 2018, this volume
 Harper, G., O’Riain, N., Ayres, T. 2013, MNRAS, 428, 2064
 Lim, J., Carilli, C., White, S., Beasley, A., Marson, R. 1998, Nature, 392, 575
 Linford, J., Chomiuk, L., & Rupen, M. 2018, this volume
 Matthews, L. & Claussen 2018, this volume
 Matthews, L., Reid, M., Menten, K. 2015, ApJ, 808, 36
 McKinnon, M. et al. 2016, SPIE, 9906, 27
 Monnier, J. et al. 2007, Science, 317, 342
 Monnier, J. 2003, Reports on Progress in Physics, 66, 789
 Montarge, M., Norris, R., Chiavassa, A. et al. 2018, A& A, 614, 12
 Mozurkewich, D., Armstrong, J., Hindsley, R. et al. 2003, AJ, 126, 2502
 Ochsenein, F., Bischoff, M. & Egret, D. 1981, A& A Supp, 43, 259
 O’Gorman E. et al. 2013, AJ, 146, 98
 O’Gorman, E. et al. 2015, A& A, 580, 101
 O’Gorman, E. et al. 2017, A& A, 602, L10
 Osten, R., Crosley, M., Gudel, M. et al. 2018, Report for National Academy of Science Committee on Exoplanet Science Strategy
 de Pater, I., Sault, R., Butler, B. et al. 2016, Science, 352, 1198
 Perryman M.A.C., Lindgren L., Kovalevsky J. et al. 1997, A& A, 323, L49
 Selina, R. & Murphy, E. 2017, ngVLA Memo. No. 17
 Triglio, C., Umana, G., Cavallaro, F. et al. 2018, MNRAS, in press
 Villadsen, J., Hallinan, G., Bourke, S. et al. 2014, ApJ, 788, 112
 Vlemmings, W., Khouri, T., O’Gorman, E. et al. 2017, NatAs, 1, 848
 White, J., Aufdenberg, J., Boley, A. et al. 2018, ApJ, 859, 102
 White, S.M., Iwai, K., Phillips, N. et al. 2017, Solar Phys, 292, 88